MODELING THE REALISTIC RIM OUTLINES OF FRESH LUNAR CRATERS BASED ON THEIR POWER SPECTRAL DENSITIES. J. Du, D. A. Minton, and A. M. Blevins, Department of Earth, Atmospheric, and Planetary Sciences, Purdue University, West Lafayette, IN 47907, USA (jundu@purdue.edu).

Introduction: Impact craters on the Moon are formed by the collision of a meteorite with the lunar surface, and the crater morphology can provide information on both projectile (e.g., diameter, velocity, and impact angle) and target (e.g., strength, porosity and gravity) properties [1]. Early studies of crater morphology focused on the diameter-dependence of morphometric parameters such as crater depth and rim height [2]. More recently, several three-dimensional shape models of fresh lunar craters were developed as the initial condition to simulate the topographic evolution of the lunar surface [3]. These three-dimensional shape models, however, always assume an axis-symmetric geometry for the crater morphology, and therefore they fail to reproduce the detailed texture of the cratered surface.

In comparison to directly modeling a lunar crater in the spatial domain, the power spectral density of its geometry in the frequency/wavelength domain has presented a great potential to reproduce its topographic variation at different wavelengths [4–6]. In this study, we demonstrate how to create the realistic rim outlines for fresh lunar craters using their power spectral densities and discuss what information can be extracted from the shape of crater rims.

Power Spectral Density of the Rim Outline: We started by selecting 78 craters (D=1–130 km) with a crisp rim, blocky surface and simple geologic context as our candidate fresh craters [7]. Then, their crater rims were vectorized by tracking the highest elevations along the rim crest in the SLDEM topographic data. Assuming a spherical geometry, the radial distance between the vertex on the rim crest and the crater center was later calculated as a function of the accumulative chord length between two vertices (Fig. 1a). The power spectral density of the rim outline was therefore calculated as [8]:

$$S = |2 \times \mathcal{F}(r)|^2 / L \quad (1)$$

where S is the power spectral density, r is the radial distance between rim vertex and crater center, L is the rim perimeter, and $\mathcal{F}$ denotes the Fourier transform.

Taking the rim of crater Copernicus (D=93 km) as an example, it can be seen that its power spectral density first increases with increasing topographic wavelength with a power-law slope of ~4, then reaches a plateau within 20–160 km, and finally drops rapidly at the longest wavelength (i.e., the rim perimeter L) (Fig. 1b). In order to characterize the overall trend of this power spectral density, four breakpoints can be placed at the resolution limit (the rim perimeter divided by the number of vertices), the onset of the plateau, the second-to-last point

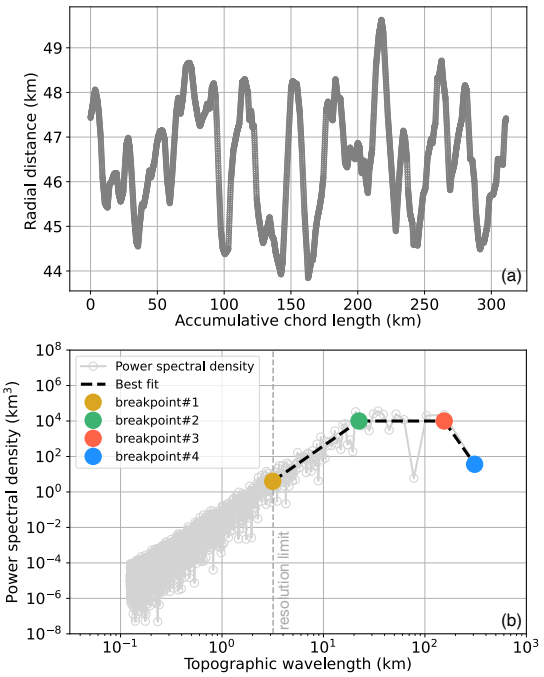

Fig. 1. (a) Radial distance between rim vertex and crater center as a function of accumulative chord length for crater Copernicus. (b) Power spectral density of the rim outline of crater Copernicus, where the four breakpoints and the best fit are shown.

(at half of the rim perimeter L/2) and the last point. Note that since the resolution limit depends on the number of vertices, which is different for each vectorization, we later used the slope between the first and second breakpoints to characterize the variation of the power spectral density between them.

In this manner, the power spectral density of each fresh crater was fitted by using four breakpoints with the least summed square of misfit. Next, the wavelength and

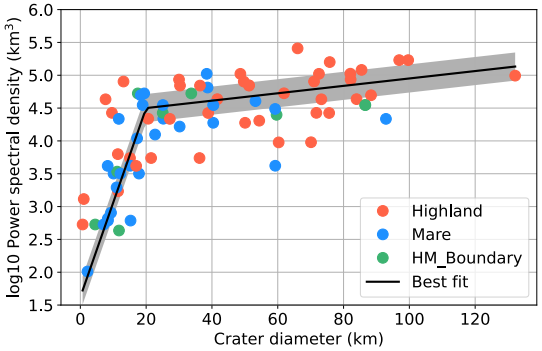

Fig. 2. Power of the third breakpoint as a function of crater diameter.

power (i.e., x and y values) of the breakpoint as well as the slope between the first two breakpoints were fitted with respect to the crater diameter. It was then found that the powers of the three breakpoints all increase with crater diameter but with a distinct change in slope at the transition of simple to complex craters (D=~20 km) [2], as is shown for the power of the third breakpoint in Fig. 2.

Reconstruction of the Rim Outline: With a given crater diameter, we can then predict the wavelength and power of the four breakpoints based on the breakpoint/slope-diameter relations (e.g., Fig. 2). Next, we connected the four breakpoints with straight lines in the *log-log* space, to which Gaussian random noises were added (gray dots in Fig. 3) to mimic the variation in the power spectral density of the crater rim (Fig. 1b). The standard deviation of these Gaussian random noises is the average root-mean-squared misfit obtained when fitting the power spectral densities of the rim outlines of fresh craters. If the rim outline is reconstructed with N vertices, its power spectral density should have $N/2$ components according to the Nyquist sampling law. Each component in the synthetic power spectral density (gray dots in Fig. 3) should correspond to a sine wave in the spatial domain, of which the amplitude and period are determined by the power and wavelength of each component. In the end, the rim outline can be reconstructed by summing those sine waves as:

$$r = \sum_{i=1}^{N/2} \sqrt{\frac{S_i \times L}{N^2}} \times \sin\left[2\pi/\left(\frac{L}{i}\right) \times (l + l_{\text{rand}})\right] \quad (2)$$

where N is the number of vertices, S_i is the power spectral density at the topographic wavelength L/i, l is the accumulative chord length, and l_{rand} is a random number with a uniform distribution between 0 and L/i, which guarantees that the newly generated rim outline is different each time.

We then evaluated how the power of the breakpoint changes the shape of the rim outline in the spatial domain. Using the power of the third breakpoint as an example (Fig. 2), it represents the amplitude of a sine wave with a

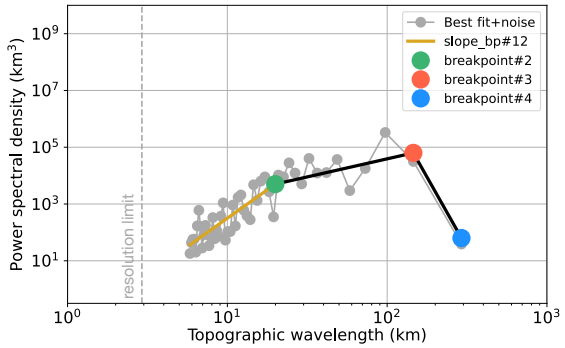

Fig. 3. Synthetic power spectral density used to reconstruct the rim of a Copernicus-sized crater. The breakpoints and the slope between the first two breakpoints are shown.

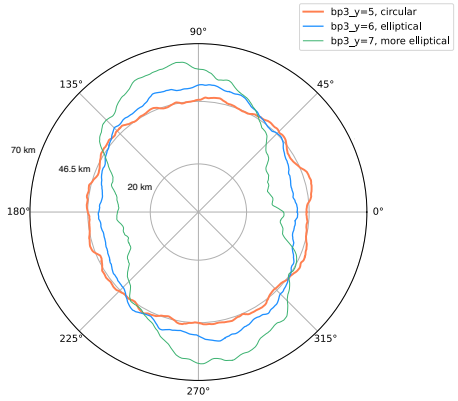

Fig. 4. Rim outlines of a Copernicus-sized crater generated with different powers of the third breakpoint (i.e., bp3_y).

period of half of the rim perimeter. For a Copernicus-sized crater, if the power of the third breakpoint increases from a normal value of 10^5 to atypical values of 10^6 and 10^7, this would result in more and more elliptical crater rims (Fig. 4). This is to be expected, since an ellipse is always axis-symmetric with respect to its major/minor axis and thus has a strong power at half of the perimeter.

Implications for the Simple-to-complex Transition of Lunar Craters: As the crater diameter increases, the morphology of lunar craters changes from a simple bowled shape to having more complex appearances such as a scalloped rim (Fig. 4), wall terraces, flat floor, and a central peak [1]. A transitional crater is defined as having one or a few of those complex features, but not all of them [1]. In the spatial domain, the diameter of such a transitional crater can be identified in the relation between morphometric parameters (e.g., crater depth and rim height) and crater diameter, which usually occurs at D=15–20 km [2]. Whereas in the wavelength domain (Fig. 2), the distinct slope change in the breakpoint power-crater diameter relation at D=~20 km also points to the transition from simple to complex craters. This provides a new way to define the diameter of transitional craters, which can also be applied to craters on other planetary bodies.

Conclusions: We modeled the rim outline of fresh lunar craters based on their power spectral densities, and found that the simple-to-complex transition of lunar craters can also be identified in the power spectral density of the rim outline. Future studies will focus on modeling other morphologic features (e.g., crater floor and continuous ejecta) using similar techniques.

References: [1] Melosh H. J. (1989) *Oxford Univ. Press, New York,* 14–22, 112–113. [2] Pike R. J. (1977) *Pergamon Press, New York*, 489–509. [3] Minton D. A. et al. (2019) *Icarus, 326,* 63–87. [4] Minton D. A. et al. (2020) *Planet. Crater Consort. XI,* Abstract #2068. [5] Watters W. A. et al. (2017) *Icarus 286*, 15–34. [6] Eppler D. T. et al. (1983) *GSA Bull. 94(2)*, 274–291. [7] Losiak A. et al. (2015) *LPI Lunar Exploration Summer Interns*. [8] Jacobs T. D. B. et al. (2017) *Surf. Topogr.: Metrol. Prop., 5,* 013001.